Journal of Ecology

Climate, soil mineralogy, and mycorrhizal fungi influence soil organic matter fractions in eastern US temperate forests

Journal:	*Journal of Ecology*
Manuscript ID	JEcol-2022-0869
Manuscript Type:	Research Article
Date Submitted by the Author:	20-Oct-2022
Complete List of Authors:	Lang, Ashley; Indiana University, Department of Biology Pett-Ridge, Jennifer; Lawrence Livermore National Laboratory, Physical and Life Sciences Directorate; University of California Merced, Life & Environmental Sciences Department Mcfarlane, Karis; Lawrence Livermore National Laboratory, Center for Accelerator Mass Spectrometry Phillips, Richard; Indiana University, Department of Biology
Key-words:	Plant–soil (below-ground) interactions, temperate forests, soil carbon, mycorrhizal fungi, global change, soil nitrogen, mineral associated organic matter, soil organic matter

Climate, soil mineralogy, and mycorrhizal fungi influence soil organic matter fractions in eastern US temperate forests

Ashley K. Lang[1*], Jennifer Pett-Ridge[2,3], Karis J. McFarlane[4], Richard P. Phillips[1]

[1]Department of Biology, Indiana University, 1001 E 3rd St, Bloomington, IN, USA

[2]Physical and Life Sciences Directorate, Lawrence Livermore National Laboratory, Livermore, California, USA

[3]Life & Environmental Sciences Department, University of California Merced, Merced, CA, USA

[4]Center for Accelerator Mass Spectrometry, Lawrence Livermore National Laboratory, Livermore, CA, USA

*corresponding author: al40@iu.edu

Abstract

1. Identifying the primary controls of particulate (POM) and mineral-associated organic matter (MAOM) content in soils is critical for determining future stocks of soil carbon (C) and nitrogen (N) across the globe. However, drivers of these soil organic matter fractions are likely to vary among ecosystems in response to climate, soil type, and the composition of local biological communities.
2. We tested how soil factors, climate, and plant-fungal associations influenced the distribution and concentrations of C and N in MAOM and POM in seven temperate forests in the National Ecological Observatory Network (NEON) across the eastern

United States. Samples of upper mineral horizon soil within each forest were collected in plots representing a gradient of dominant tree-mycorrhizal association, allowing us to test how plant and microbial communities influenced POM and MAOM across sites differing in climate and soil conditions.

3. We found that concentrations of C and N in soil organic matter were primarily driven by soil mineralogy and climate, but the relative abundance of MAOM *vs.* POM C was strongly linked to plot-level mycorrhizal dominance. Further, the effect of dominant tree mycorrhizal type on the distribution of N among POM and MAOM fractions was sensitive to local climate: in cooler sites, an increasing proportion of ectomycorrhizal-associated trees led to lower proportions of N in MAOM, but in warmer sites, we found the reverse. As an indicator of soil carbon age, we measured radiocarbon in the MAOM fraction, but found that within and across sites, $\Delta^{14}C$ was unrelated to mycorrhizal dominance, climate, or soil factors, suggesting that additional site-specific factors may be primary determinants of long-term SOM persistence.
4. **Synthesis**: Our results indicate that while soil mineralogy and climate primarily control SOM C and N concentrations, the distribution of SOM among density fractions depends on the composition of vegetation and microbial communities, with these effects varying across sites with distinct climates. We also suggest that within biomes, the age of mineral-associated soil carbon is not clearly linked to the factors that control concentrations of MAOM C and N.

Introduction

Given the vast size of the global carbon (C) pool (Scharlemann et al., 2014), and the desire to promote additional soil C storage, the factors that control the persistence of soil C are of

critical concern (Amelung et al., 2020; Bossio et al., 2020; Lal, 2004; Paustian et al., 2019). However, not all components of soil organic matter (SOM) have an equal potential to influence carbon-climate feedbacks, as certain soil pools are often more vulnerable to decay and removal than others (K. Heckman et al., 2022; Torn et al., 1997). Roughly two-thirds of terrestrial organic C is contained in mineral soils as either particulate organic matter (POM) or mineral-associated organic matter (MAOM; (Sokol et al., 2022). Formed from partly-decayed plant and faunal biomass, POM is often characterized as vulnerable to continued decomposition, but remains a critical pool of nutrients and carbon in ecosystems where decomposition rates are limited either by climate or the chemical complexity of POM (Haddix et al., 2020; Lugato et al., 2021). In contrast, MAOM is composed of organic compounds that are associated with minerals through physical and chemical bonds (Lehmann & Kleber, 2015; Sokol et al., 2018), which may confer some protection against microbial access and further decomposition (Lugato et al., 2021). MAOM is therefore a potentially important long-term reservoir of soil C, and there have been many efforts to quantify and characterize MAOM in ecosystems across the globe.

The primary environmental conditions that explain POM and MAOM pool sizes vary widely across study systems (Craig et al., 2022; Haddix et al., 2020; K. Heckman et al., 2022; Mikutta et al., 2019; Sokol et al., 2022), suggesting that there may be context-specific soil conditions and biological communities that influence their formation and persistence. Suggested drivers of POM and MAOM formation in soil include the quantity and chemistry of organic matter inputs from roots and aboveground litter (Cotrufo et al., 2013; Craig et al., 2022; Crow et al., 2009; Keller et al., 2021), microbial community composition and activity (Cotrufo et al., 2019; Craig et al., 2018; Frey, 2019; Sokol et al., 2022; Sollins et al., 2009), and soil texture and mineralogy (K. A. Heckman et al., 2015; Kögel-Knabner et al., 2008; Schöning et al., 2005;

Sollins et al., 2009; Swenson et al., 2015; Torn et al., 1997; Weng et al., 2018). Further, local climate may govern the strength of these drivers across ecosystems (Kramer & Chadwick, 2018). Given this lack of consensus and the wide variation in the spatial influence of these drivers, it is likely that cross-scale interactions (*sensu* Soranno et al., (2014)) between soil mineralogy, microbial communities, and organic matter quantity and quality collectively determine MAOM pool sizes, wherein the strength of each factor in a particular ecosystem is dependent on the underlying characteristics of the ecosystem. For example, the availability of mineral surfaces for organic matter sorption may serve as a primary determinant of the MAOM formation potential of an ecosystem, and plant or microbial community composition might therefore influence MAOM formation only where the soil mineral composition is suitable for organic matter sorption (Jones et al., 2015; Kögel-Knabner et al., 2008; Mikutta et al., 2019; Slessarev et al., 2022). This context-dependency is common among drivers of large-scale ecosystem processes (Catford et al., 2022; Hakkenberg et al., 2021; Tedersoo et al., 2016), including soil organic matter dynamics (Hoffland et al., 2020; Kramer & Chadwick, 2018; Rasmussen et al., 2018), reinforcing the need to test these interactions across scales (Nave et al., 2021).

Plant-mycorrhizal associations can also drive within-ecosystem variation in soil C and N cycling and affect the distribution of organic matter as POM and MAOM, particularly in forests. Recent work indicates that in temperate forests where the majority of trees associate with arbuscular mycorrhizal (AM) fungi *vs.* ectomycorrhizal (ECM) fungi, more of the total soil C is stored as MAOM rather than POM (Cotrufo et al., 2019; Craig et al., 2018). This pattern has been attributed to covarying traits of AM and ECM-associated tree species, such as the typically higher decay rates of AM-associated tree leaf litter (Keller & Phillips, 2019), and to the higher rate of root-derived organic matter inputs in AM-dominated forests (Keller et al., 2021).

Therefore, in AM-dominated stands, fast-decomposing litter and large belowground inputs of labile C may stimulate microbial activity and turnover and lead to faster MAOM production than is observed in ECM-dominated stands (Craig et al., 2018). Further, differences in the productivity and activity of mycorrhizal fungi themselves, including hyphal production and turnover, and exoenzyme production and organic matter decay, may also influence the formation and stability of POM and MAOM (Frey, 2019). Regardless of the mechanism for MAOM formation in ecosystems with distinct mycorrhizal types, it is unclear whether this pattern—larger proportions of C in MAOM under AM *vs* ECM trees—is consistent across forest types or dependent on local climate and soil mineralogy.

Despite the generally longer residence time of MAOM compared with POM (K. Heckman et al., 2022; Swanston et al., 2005), observations of rapid MAOM formation and destabilization under conditions representative of rhizosphere soil suggest that MAOM is composed of some fast-cycling organic matter and some older, more tightly bound organic matter (Fossum et al., 2022; K. A. Heckman, Swanston, et al., 2021; Jilling et al., 2021; Keiluweit et al., 2015; Neurath et al., 2021; Swanston et al., 2005). Because MAOM persistence is dictated both by rates of formation and destabilization, concentrations of MAOM C and N in soil do not necessarily reflect MAOM persistence. The potential for MAOM destabilization may be primarily determined by the same factors that influence MAOM formation, including conditions in the soil matrix (Kramer & Chadwick, 2018; Waring et al., 2020) or the particular features of the organo-mineral associations by which MAOM is formed, including both the type and crystallinity of soil minerals as well as the chemical and physical structure of the organic compounds (K. Heckman et al., 2018; Kögel-Knabner et al., 2008). Alternatively, MAOM persistence may be driven by a separate suite of ecosystem properties than MAOM formation,

including the rate of organic acid production and carbon exudation by roots and microbes (Jilling et al., 2021; Keiluweit et al., 2015), decoupling the rates of formation and destabilization and leading to patterns in MAOM persistence dictated by local conditions.

To assess the strength of mineralogical, biological, and climatic drivers of POM and MAOM C and N content and MAOM C persistence in soils across the eastern U.S., we analyzed soil collected from plots representing gradients of tree-mycorrhizal associations within seven forested sites in the National Ecological Observatory Network (NEON) that span a range of climate conditions and vary in soil mineralogy. We then compared the roles of climate, soil oxalate-extractable iron content, and mycorrhizal dominance (% basal area of trees associating with either AM or ECM fungi) in driving POM and MAOM C and N concentrations, the distribution of soil C and N among POM and MAOM fractions, and measured $\delta^{13}C$ and $\Delta^{14}C$ to assess the mechanisms of MAOM C formation and persistence. We hypothesized that tree-mycorrhizal associations would influence the distribution of C and N among the POM and MAOM fractions, but that the effect of dominant tree mycorrhizal type on MAOM and POM would be smaller than the effects of soil mineralogy and climate. Further, we expected that higher concentrations of MAOM C and N would generally correspond with longer MAOM residence times (estimated using MAOM $\Delta^{14}C$) and a higher degree of microbial processing (i.e. higher $\delta^{13}C$) in forest soils, but that this relationship may be dependent on climate.

Materials and methods

Soil sampling

We obtained mineral horizon soil samples from study plots located within seven forests in the National Ecological Observatory Network (Figure 1) from the NEON Biorepository at

Arizona State University (https://biorepo.neonscience.org/portal/). Soil samples were collected during the growing season between 2014 and 2020 following standard NEON protocols (Hinckley et al., 2016). Samples were collected from the upper 30 cm of the soil profile, unless rocks or other site characteristics prevented coring to this depth; in such cases, the maximum accessible depth was used. Within each plot, cores were collected in a number sufficient to provide the necessary soil mass for chemical and physical analyses. Organic and mineral horizon soils were separated, and in cases where multiple cores were collected within a plot, samples were aggregated and homogenized by horizon to represent the soil conditions at the plot scale. Samples were air-dried and sieved to 2mm prior to archiving. Forest sites were chosen for this study based on the availability of physical soil samples suitable for representing within-site variation in tree mycorrhizal type (for site descriptions, see Table 1). Plots within each site (TREE: n=6, all others: n=7) were selected to represent the largest possible range of dominance by AM- vs. ECM-associated tree species at the plot level within each site (Figure 1b).

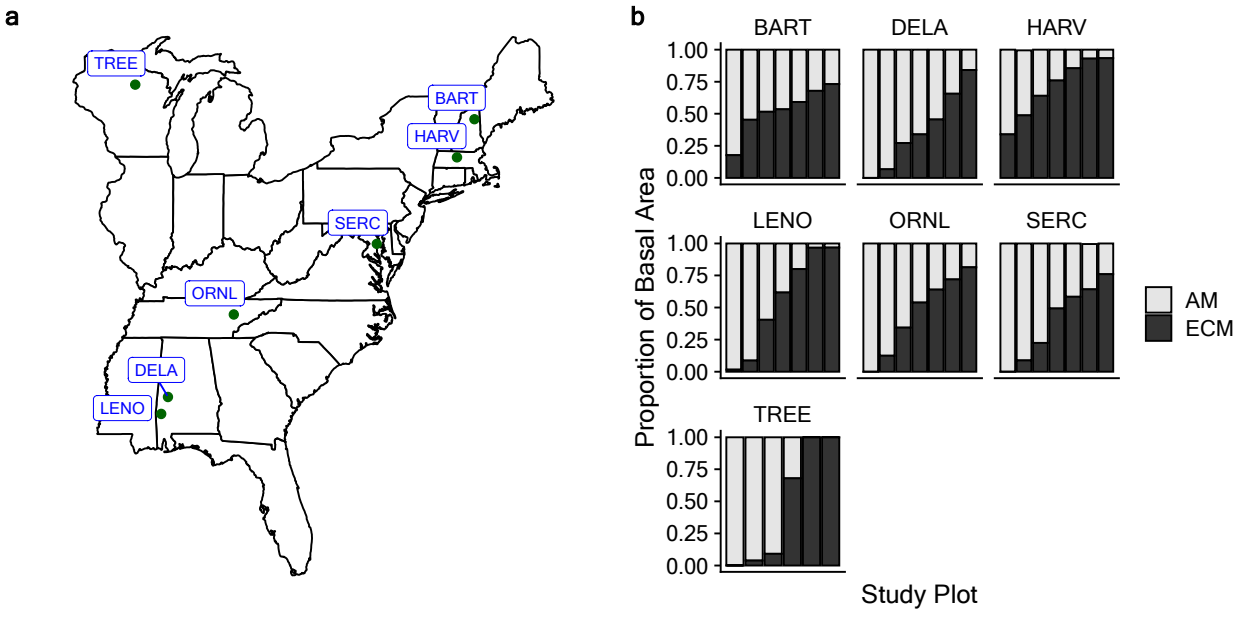

Figure 1. (a) Locations of seven NEON temperate forest sites used in this study (b) Proportion of basal area attributed to arbuscular mycorrhizal (AM)- and ectomycorrhizal (ECM)-associated tree species within the plots where soil was collected in each site.

Data selection and processing

The mycorrhizal dominance (i.e. %ECM and %AM tree basal area) of each study plot was calculated using tree basal area and species identity data from the Vegetation Structure data set on the NEON Data Portal (NEON, 2022b). To assess tree species composition, we used woody vegetation data for the most recent year of sampling at the time of data download from each study site, excluding years where sampling efforts were interrupted by external factors or where data collection was otherwise incomplete. We filtered these data to include only live individuals with measurements of stem diameter and with either a species or genus level identification. Woody vines were excluded from the dataset. Mycorrhizal association of each species was determined using the USDA PLANTS database (USDA, NRCS. National Plant Data Team., 2021), and plot-level AM and ECM dominance was calculated by dividing the total basal area of all AM-associated trees and all ECM-associated trees from the total basal area in each plot. Where tree species were not known, we used genus to assign dominant mycorrhizal type to individual stems. Trees associated with ericoid mycorrhizal fungi were present in eight of the study plots, and constituted no more than ~0.5% of the basal area in any one plot (Table S1). To assess associations between tree mycorrhizal type and leaf litter production, we used data from the Litterfall and fine woody debris production and chemistry data set from the NEON data portal (NEON, 2022a). These data were filtered to include only leaf and needle litter, and only data collected in the most recent years when sampling was not disrupted by external factors to maximize the available dataset. These years ranged from 2016 to 2019. Mean annual litterfall mass for each study plot was calculated as the mean value of the annual sum of all leaf and

needle litter mass from each study plot. NEON datasets were accessed and merged using the neonUtilities package in R (Lunch et al., 2021).

Soil chemical analyses

We separated air-dried mineral soil samples into particulate and mineral-associated forms of organic matter with density fractionation (Sollins et al., 2009) using sodium polytungstate (SPT) adjusted to a density of 1.7 g/mL. Briefly, approximately 5 g of mineral horizon sample was submerged in SPT solution and centrifuged to isolate loose, floating organic material (hereafter the free particulate organic matter [fPOM] fraction). Then, particulate matter contained within soil aggregates was separated from the remaining material by shaking the sample to disrupt aggregates for 18 hours at 200 oscillations per minute on a shaker table and centrifugation to isolate material with a density less than 1.7 g/mL (hereafter the occluded particulate organic matter [oPOM] fraction). The remaining organic matter was considered mineral-associated organic matter (hereafter MAOM). Following separation, all organic matter fractions were rinsed of residual SPT using Nanopure water, oven dried, and analyzed for percent carbon and nitrogen using an elemental combustion system (Costech Analytical Technologies, Valencia, CA, USA). The SPT solution was standardized to a density of 1.7 g/mL for all samples, which was deemed sufficient for clear separation of SOM pools with centrifugation following visual inspection.

Isolated MAOM from mycorrhizal gradient plots in six of the NEON sites was analyzed for $\delta^{13}C$ and $\Delta^{14}C$. Samples were analyzed for $\delta^{13}C$ at the Stable Isotope Research Facility in the Department of Earth and Atmospheric Sciences at Indiana University. Samples were run on an elemental combustion system (Costech ECS 4010, Costech Analytical Technologies, Valencia,

CA, USA) attached to an isotope ratio mass spectrometer (Thermo Finnigan DELTA Plus XP IRMS; San Jose, CA, USA) with a gas bench interface. $\Delta^{14}C$ measurements were conducted at the Center for Accelerator Mass Spectrometry at Lawrence Livermore National Laboratory (as per McFarlane, et al. 2013). Samples were not pre-treated to remove carbonates due to the relatively acidic conditions observed in soils from these sites; mean soil pH in each site ranged from 4.33 (BART) to 5.54 (DELA). Samples from ORNL were not included in isotope analyses due to ^{14}C contamination from a nearby hazardous waste incinerator (Trumbore et al., 2002). Samples were combusted and converted to graphite (Vogel 1984) and analyzed on the NEC 1.0 MV Tandem Accelerator Mass Spectrometer (Broek et al., 2021). The ^{14}C content of each sample was reported in $\Delta^{14}C$ notation, corrected for mass-dependent fractionation with measured $\delta^{13}C$ values, and then corrected to the year of measurement (2021) for ^{14}C decay since 1950 (Stuiver & Polach, 1977).

To determine oxalate-extractable iron content, a 0.2 g subsample of bulk mineral soil from each study plot was submerged in 20 mL of a 0.2 M oxalate extracting solution, shaken at low speed for four hours in the dark, centrifuged for 15 min at 2500 rpm, and filtered through grade 1 qualitative filter paper (Whatman, Buckinghamshire, UK). Extracts were then analyzed for iron content on a mass percent basis with atomic absorption spectrometry (PerkinElmer Instruments, Waltham, MA, USA).

Climate Decomposition Index

We extracted monthly temperature and precipitation data for each NEON site for the year 2017 using the Parameter-elevation Regressions on Independent Slopes Model (PRISM) dataset (PRISM Climate Group, Oregon State University, n.d.). We then calculated the climate

224 decomposition index (CDI) of each site to represent the overall climate using the temperature
225 functions described by Lloyd and Taylor (1994) following Adair et al. (2008). The CDI of each
226 site is a function of minimum and maximum monthly temperature and monthly precipitation, and
227 represents an integrated index of conditions important for influencing decomposition. Higher
228 CDI values indicate warmer or wetter sites; for the seven forests studied here, mean annual
229 precipitation was less variable than mean annual temperature, so CDI values primarily reflect
230 differences in site temperature.
231
232 *Statistical analysis*
233 To address our hypothesis that climate, soil mineralogy, and mycorrhizal dominance
234 influence SOM interactively, we constructed a suite of linear models for the proportions of total
235 soil C and N stored in each density fraction as well as the concentrations of MAOM and POM C
236 and N per gram of mineral soil. These models include plot-level mycorrhizal dominance and soil
237 FeOx content and site-level CDI as fixed effects, with study site as a random intercept (Bates et
238 al., 2015). Because we expected the effects of these variables to change across climate and soil
239 conditions, we also tested all pairwise interactions between our fixed effects, but included
240 interaction terms in the final models only when they significantly influenced SOM fractions.
241 Finally, we compared models of MAOM C and N content using each site's mean annual
242 temperature in place of CDI; both methods yielded the same patterns, so we present models
243 using CDI to represent variability in both temperature and precipitation across sites. One sample
244 from Harvard Forest (HARV) with an exceedingly high value of fPOM C and N concentration (>
245 20 standard deviations above mean fPOM C concentration; > 6 standard deviations above mean
246 fPOM N concentration) was removed from these analyses for a total of 47 observations.

Additionally, we constructed linear models with the same fixed and random effects to test how the C:N of each density fraction, as well as the $\delta^{13}C$ and $\Delta^{14}C$ of the MAOM fraction, responded to mycorrhizal associations, FeOx content, and climate. We also used a series of simple linear models to assess whether the MAOM C concentrations or the proportions of C in the MAOM fraction were associated with MAOM C isotope ratios. Linear mixed effects models were constructed with the lme4 package in R (v. 4.0.2) (Bates et al., 2015).

To further investigate how patterns in leaf litter production may have influenced our results, we constructed simple linear models of leaf litter mass across AM-ECM tree gradients within each NEON study site. For this analysis, we gathered data from all plots for which appropriate litter mass data were available from the NEON data portal; therefore, these plots do not necessarily correspond to those from which we were able to request soil samples for density fractionation, instead representing the general patterns in litter production with respect to tree mycorrhizal associations within each site.

Results

Distribution of soil C and N among density fractions

To test our hypothesis that tree mycorrhizal associations influence the formation of POM and MAOM, we assessed how the proportion of C and N in MAOM vs POM varied with the dominant mycorrhizal type of the trees in our study plots. The mean percentage of total soil C [80 ± 1.1 %] and N [89 ± 0.9] contained in the MAOM fraction was generally consistent across study sites, but varied within sites along gradients of AM to ECM tree dominance in the forest plots (Table 2). With increasing ECM-associated tree basal area, we found that the proportion of C in particulate fractions (both fPOM and oPOM) increased (fPOM: $t_{41}= 2.21$, $p= 0.033$; oPOM:

t_{41}= 2.30, p= 0.027), and in turn, the proportion of C in MAOM decreased (t_{41}= -3.29, p= 0.002) within the majority (6 out of 7) of our study sites (Figure 2). In one site (LENO), we observed the opposite pattern, where a higher proportion of C in the MAOM was associated with increasing ECM tree dominance ($F_{1,5}$=6.554, p= 0.0506). However, combining all sites, the mean percentage of total soil C in the MAOM fraction decreased by 8.0% across a gradient of 100% AM to 100% ECM tree basal area.

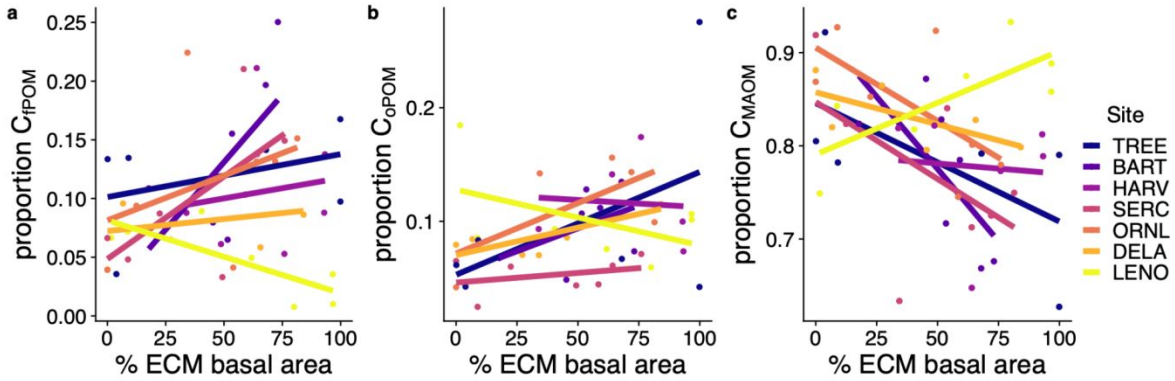

Figure 2. Proportions of total soil C in the a) free particulate fraction (C_{fPOM}), b) occluded particulate fraction (C_{oPOM}, and c) mineral-associated organic matter (C_{MAOM}) fraction in plots situated along a gradient of tree mycorrhizal dominance in seven forested NEON sites (see Table 1 for site definitions). Points represent individual plots within each study site (n=46). Lines reflect the best fit from linear models specific to each study site.

The proportion of soil N in the MAOM fraction responded differently to mycorrhizal dominance under different climate conditions (t_{40}= 2.17, p= 0.036; Table 2); in cooler sites, the proportion of soil N in the MAOM fraction declined with increasing dominance of ECM-associated tree species, but increased with ECM dominance in warmer sites (Figure 3). The proportion of N in the oPOM fraction showed the reverse, with stronger positive relationships with ECM

dominance in colder sites (t_{40}= -2.17, p= 0.036; Table 2). To better assess how differences in organic matter inputs may have influenced the patterns we observed along AM to ECM-dominated gradients, we compared leaf and needle litter production with tree mycorrhizal type in all seven forests; the dry mass of leaf and needle litter was negatively associated with plot-level ECM tree dominance in only two sites: TREE ($F_{1,18}$= 22.65; p < 0.001) and BART ($F_{1,18}$= 8.95; p = 0.008).

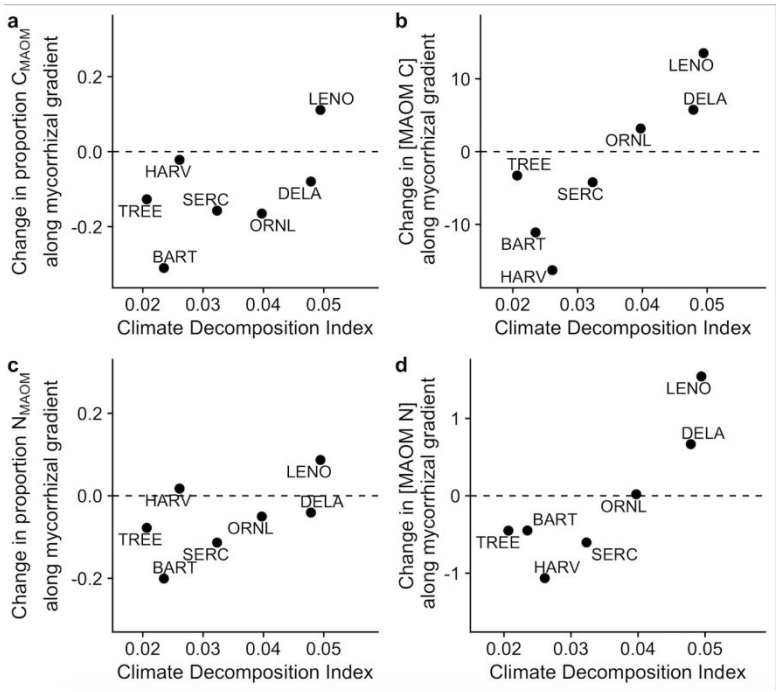

Figure 3. The influence of tree mycorrhizal dominance (%ECM tree basal area) on MAOM C (a-b) and N (c-d) proportions and concentrations in seven forested NEON sites with respect to climate decomposition index (CDI). CDI represents the mean values and variability of monthly temperature and precipitation in each site (see Methods for details and calculation). Each point represents the slope of the relationship between MAOM C or N and plot-level ECM dominance within a site (as in Figure 2). Panels a and c show the strength and direction of changes in the proportion of C and N in MAOM with increasing ECM tree dominance in each site, while panels b and d show the strength and direction of changes in the concentrations of mineral-bound C and N with increasing ECM dominance. Points above the dotted line represent positive slopes (i.e. soils in

311 *these sites show an increase in MAOM C and/or N with increasing ECM dominance; n=7 for all*
312 *sites except TREE and HARV [n=6]).*
313
314 *Mineralogical and climatic controls on SOM C and N concentrations*
315 Because soil mineralogy and climate-driven weathering are recognized as key
316 determinants of mineral-organic matter relationships (Rasmussen et al., 2018; Slessarev et al.,
317 2022), we tested how bulk soil oxalate-extractable iron (FeOx) concentration and site-level
318 climate decomposition index (CDI) influenced the distribution of C and N among soil density
319 fractions. Bulk soil FeOx concentration was strongly associated with higher concentrations of
320 MAOM C (t_{41}= 4.11, p< 0.001) and N (t_{41}= 5.88, p< 0.001 ; Figure 4) but was not an important
321 predictor of oPOM or fPOM concentrations (Table 2). Concentrations of C and N in nearly all
322 soil fractions were negatively associated with CDI; in other words, warmer sites tended to have
323 lower C and N concentrations in both POM fractions and lower MAOM C concentration (Table
324 2). FeOx concentration was also positively associated with the proportion of C in MAOM (t_{41}=
325 3.13, p= 0.003), but not with the proportion of N in MAOM (Table 2).

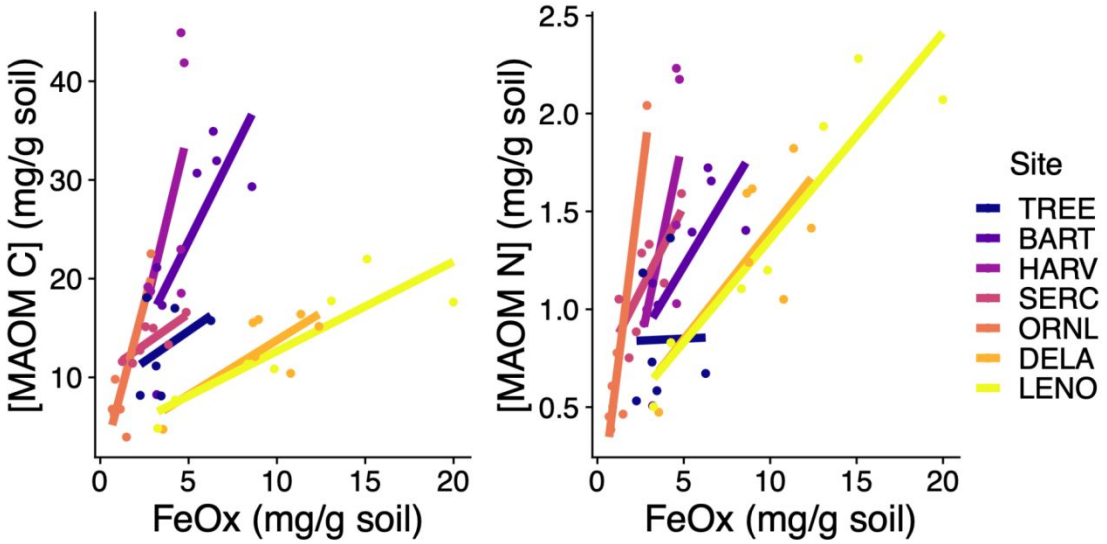

326

Figure 4. Concentrations of MAOM C and N in soils from 7 forested NEON sites (see Table 1 for site definitions) versus concentrations of oxalate-extractable iron (FeOx) in bulk surface mineral soils. Individual points represent measured values of FeOx from the same bulk mineral soil samples used to determine MAOM and POM content via density fractionation (n=46).

Patterns in SOM C:N and MAOM carbon isotopes

To better understand the pathways of MAOM formation, turnover, and SOM origin, we assessed how mineralogical, climatic, and microbial drivers impacted SOM fraction C:N and the isotopic composition of MAOM C. The C:N of all three density fractions generally increased with ECM dominance, but this effect was strongest in the POM fractions (Figure 5; Table 3). In addition, MAOM C:N was significantly lower in warmer sites (t_{41}= -4.42, p< 0.001), while neither the fPOM nor oPOM fraction was associated with site climate (Table 3). Finally, the fPOM C:N was negatively associated with FeOx concentration (t_{41}= -2.62, p= 0.012; Table 3).

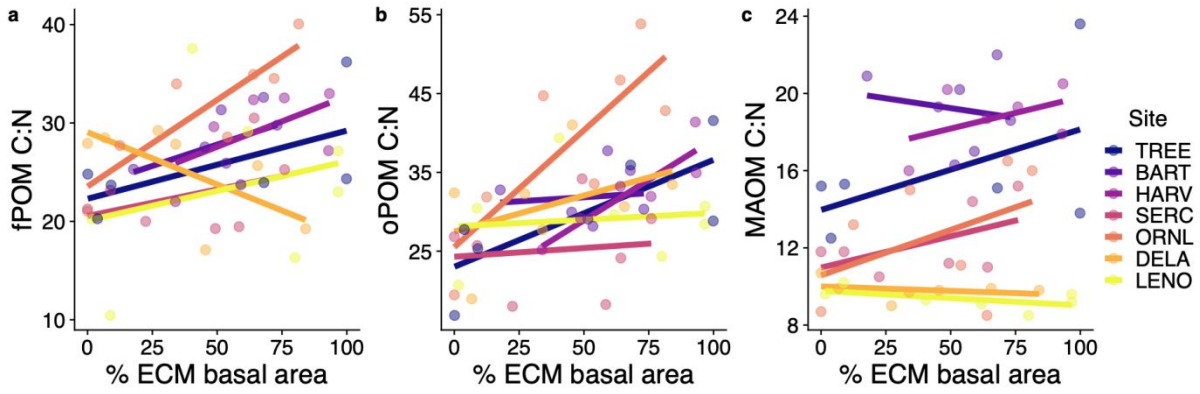

Figure 5. SOM C:N in soils from 7 forested NEON sites (see Table 1 for site abbreviations) along gradients of tree-mycorrhizal associations ranging from AM-dominated to ECM-dominated forest plots within each site. Individual points represent measured ratios of carbon to nitrogen in density fractionated fPOM, oPOM, and MAOM samples (n=47).

We measured radiocarbon content of the MAOM fraction as an estimate of the carbon age to illuminate possible drivers of MAOM persistence. The $\Delta^{14}C$ of the soil MAOM fraction varied substantially across six of the forest sites (ORNL omitted from this analysis due to environmental ^{14}C contamination; Figure 6; Table 4) but was not correlated with any of the soil, climate, or plant-fungal variables that we tested (Figure S1), nor was it related to the MAOM C concentrations ($F_{1,39}$= 0.215; p = 0.65) or proportions of C in MAOM ($F_{1,39}$= 0.044; p = 0.83). MAOM in most sites was near modern in origin, with the least modern C in the MAOM fraction at Dead Lake, AL (DELA) and the most modern C incorporated into MAOM at the Smithsonian Environmental Research Center (SERC). MAOM $\delta^{13}C$ signatures were positively associated with soil FeOx content, though this relationship was driven primarily by samples from Lenoir Landing, AL (LENO), which had the highest values of oxalate-extractable iron content of any site (Table 4). We also observed a negative association between climate decomposition index and MAOM $\delta^{13}C$, but the size of this effect was minimal (-0.04 ‰ across the range of CDI values represented by our sites; Figure S1). Finally, MAOM $\delta^{13}C$ signatures were not associated with either MAOM C concentrations ($F_{1,39}$= 0.004; p = 0.94) or the proportion of C in the MAOM fraction ($F_{1,39}$= 0.47; p = 0.50).

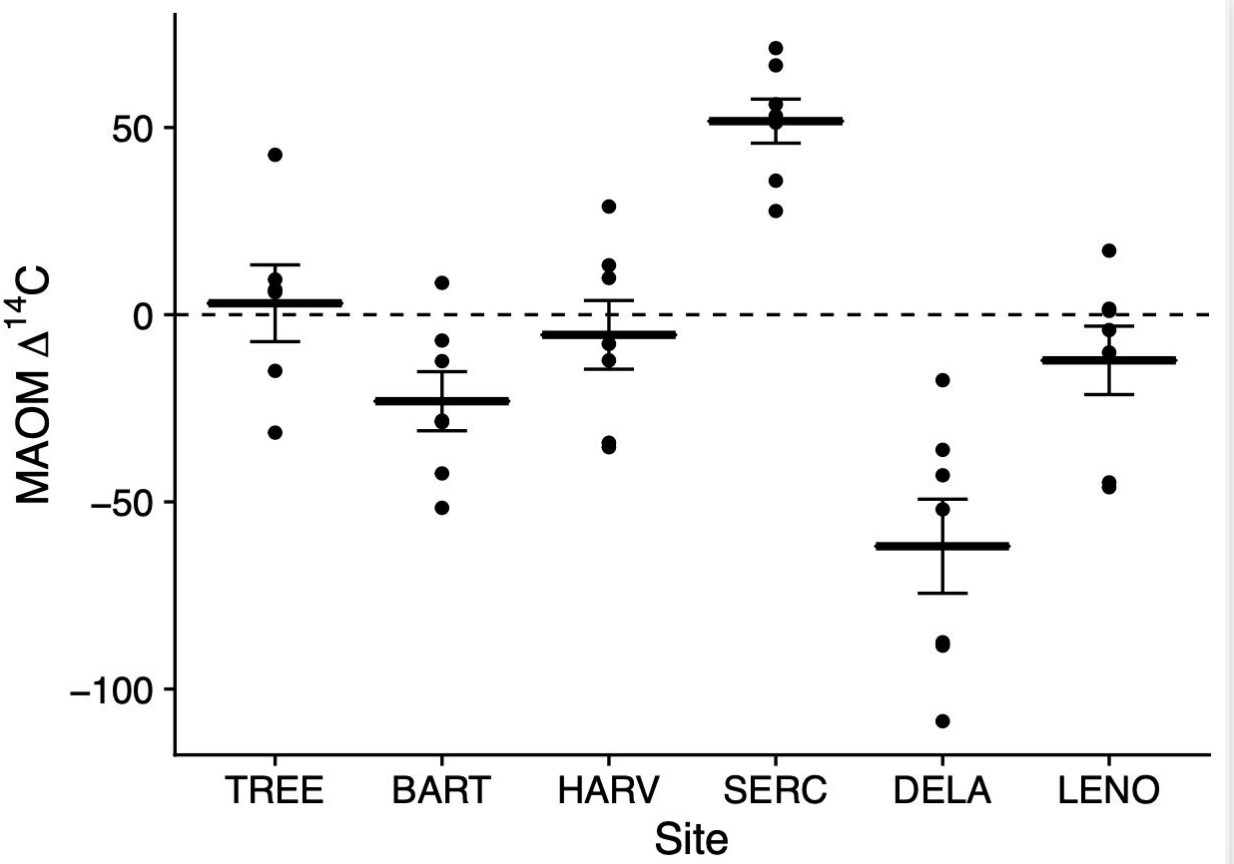

Figure 6. Mean (± SE) Delta ^{14}C of MAOM from six NEON temperate forests (ORNL was omitted due to site-level ^{14}C contamination). Values greater than zero indicate a modern origin of MAOM C with shorter turnover times; negative values indicate older C (i.e. C fixed pre-1950). Individual points represent MAOM isolated from mineral horizon soil samples (0-30 cm) collected along tree-mycorrhizal gradients within each site. Sites ordered by increasing climate decomposition index.

Discussion

Tree mycorrhizal associations influence the relative abundance of MAOM and POM C within sites

We show that the dominance of AM- *vs* ECM-associated tree species influences the relative abundance of MAOM C and POM C within eastern temperate forests: beneath AM trees, a higher proportion of the soil carbon was found in the MAOM fraction compared to the POM fraction, while the reverse was true beneath ECM trees. Notably, this pattern was consistent in all but one site (Figure 2), and the additional variance in MAOM and POM C proportions explained by other features of each site not measured in this study (i.e. the random effect of site) was small or negligible (Table S2). These results add to the body of evidence that the mycorrhizal communities present in soil may influence the likelihood that incoming organic matter becomes mineral-bound (Cotrufo et al., 2019; Craig et al., 2018). Differences between forests dominated by tree species with AM *vs.* ECM associations, in particular, may arise from variation in decomposition processes beneath AM- and ECM-associated trees. Previous studies show that both microbial community composition and activity can vary with tree mycorrhizal type (Carteron et al., 2020; Cheeke et al., 2016; Fitch et al., 2020; Moore et al., 2015; Singavarapu et al., 2022), but the extent to which these changes influence MAOM formation is difficult to test. Mycorrhizal association type is often strongly associated with related factors that are likely to impact SOM decay and sorption, including include the quality of organic matter inputs (Cornelissen et al., 2001; Huang et al., 2022; Keller & Phillips, 2019), the composition of the free-living bacterial and fungal communities (Carteron et al., 2020; Fitch et al., 2020; Singavarapu et al., 2022), and the production of organic compounds by roots and mycorrhizal fungi themselves (Keller et al., 2021).

Climate mediates the effect of mycorrhizal fungi on SOM nitrogen distribution

The effect of tree-mycorrhizal dominance on the abundance of MAOM N *vs* POM N varied across sites, implying that the role of mycorrhizal fungi in soil nitrogen dynamics is

context-dependent. Specifically, we noted that larger proportions of soil N were found in the MAOM fraction in AM-dominated forest plots in sites with cooler climates, but that in warmer sites, more of the total soil N was found in the MAOM fraction in ECM-dominated plots. One possible explanation for the differences in these patterns across sites may be that the primary origin of the mineral-bound organic matter may vary with site climate (Angst et al., 2021; Liang et al., 2019). Molecular analyses of MAOM from other NEON sites shows that MAOM in forests receiving >1200 mm precipitation annually with ratios of MAOM C to N greater than 15 may be primarily composed of plant-derived, rather than microbially-derived organic matter (Yu et al., 2022). In our study, these conditions are found at BART and HARV (Figure 5; Table 1), where we also noted that leaf litter inputs are lower in ECM-dominated plots *vs.* AM-dominated plots (Figure S1). Therefore, the decline in MAOM N concentration with ECM dominance in these sites may be partly explained by a smaller contribution of plant-derived dissolved organic matter, owing to the generally slower decomposition rate of ECM leaf litter in temperate forests (Keller & Phillips, 2019), smaller inputs of aboveground litter in ECM-dominated plots (Figure S1), or lower rates of root-derived organic matter input from ECM *vs*. AM trees (Keller et al., 2021). This explanation is broadly supported by other studies showing larger MAOM pools beneath AM versus ECM vegetation in other temperate forests (Cotrufo et al., 2019; Craig et al., 2018).

In addition to factors that influence the rate of MAOM N accumulation, destabilization and removal of N from soil mineral surfaces may also contribute to patterns in MAOM N concentrations with tree mycorrhizal type. These mechanisms may be particularly important in cooler sites where decomposition rates are lower and N limitation of primary productivity is potentially greater than in warmer sites, leading to N mining by plant roots and mycorrhizae

from mineral-bound organic matter (Jilling et al., 2018; Lambers et al., 2008; Lovett et al., 2018). Given that some species of ECM fungi have retained the ability to depolymerize organic matter as a source of N for their plant hosts (Pellitier & Zak, 2018), it is possible that N mining by ECM fungi may contribute to lower concentrations of MAOM N beneath ECM trees in cooler sites. Both of these processes—higher MAOM N inputs from AM-associated tree litter and potential removal by ECM fungal mining—may weaken in strength in warmer climates, where differences in leaf litter decay rates between AM and ECM trees are generally smaller (Keller & Phillips, 2019), and where higher POM decomposition rates may reduce the need for N mining from mineral soil as a dominant pathway of plant N uptake.

The positive relationship we found between MAOM N proportions and ECM tree dominance in the warmer sites is not as widely supported by existing literature. This relationship is particularly strong at LENO and DELA, both located in central Alabama, USA; however, the potential mechanisms behind the patterns may be distinct at these two sites. At LENO, ECM tree dominance is positively correlated with soil FeOx content, so higher concentrations of MAOM N beneath ECM trees in this site are likely due to corresponding differences in soil mineral suitability (Keiluweit et al., 2012; Swenson et al., 2015). However, soil FeOx content was not an important driver of the proportion of soil N in the MAOM fraction, and yet the fraction of N in MAOM was positively associated with ECM dominance. At DELA, it is possible that tree species exhibit preferences for other soil conditions that also correspond to tree mycorrhizal type; for example, ECM-associated trees may be abundant in wetter microsites, where decomposition is limited by seasonal inundation and water-filled pore space allows for the rapid transport of low-molecular-weight organic compounds to mineral surfaces (Waring et al., 2020). However, MAOM in these sites also had the lowest C:N ratios, indicating a greater influence of

442 microbially-derived organic matter in the mineral soil (Figure 5), and it has been suggested that
443 the proportion of microbial vs. plant-derived contributions to MAOM are positively associated
444 with mean annual temperature (Angst et al., 2021). Therefore, we suggest that in these warmer
445 sites, fungal tissues may constitute a larger proportion of the organic matter forming MAOM.
446 Given that ECM-associated trees are thought to invest more in mycorrhizal tissue production
447 than in root tissue production compared to AM-associated trees (Jevon & Lang, 2022; Tedersoo
448 & Bahram, 2019), it is therefore possible that in warmer forests, soil beneath ECM-dominated
449 stands stores more N in the MAOM fraction in part due to the turnover of chitin-rich ECM
450 fungal hyphae (Fernandez et al., 2016). If so, the primacy of fungal vs. plant-derived tissues as
451 precursors to MAOM may also account for the fact that changing MAOM N proportions with
452 increasing ECM dominance is not necessarily accompanied by changes in MAOM C proportions
453 (Table 2).
454
455 *Effects of soil mineralogy and climate on MAOM C and N*
456 Across our study sites, we found that the concentrations of MAOM C and N in soil were
457 primarily explained by soil mineralogy and climate. The concentration of oxalate-extractable
458 iron in soil (FeOx), representing the abundance of the poorly crystalline mineral phases best
459 suited for forming organo-mineral associations (Kleber et al., 2005), was the strongest driver of
460 MAOM C and N concentrations. On average, a one percent increase in soil FeOx concentration
461 led to an increase of 32 mg of MAOM C and 2.4 mg of MAOM N per gram of soil. This pattern
462 has been observed previously, strengthening the evidence that mineralogy controls MAOM
463 content despite the large variation in soil order, climate and forest species composition among
464 our sites (K. A. Heckman et al., 2015; Kögel-Knabner et al., 2008; Mikutta et al., 2006;

Slessarev et al., 2022; Torn et al., 1997; Weng et al., 2018). Further, climate strongly influenced the concentration of MAOM C. We expected that warmer or wetter conditions would accelerate litter leaching and POM decomposition, leading to faster production of the small-molecular weight compounds that form the bulk of MAOM. While this may be the case, we did not find a corresponding pattern with MAOM C concentration: instead, we found that warmer sites generally had lower overall concentrations of MAOM C (Table 2). This pattern may result from a shift in the balance of MAOM C inputs and losses with site climate. In warmer sites, where microbial activity is not as limited by cooler annual temperatures, microbes may be better able to overcome the energetic constraints of accessing MAOM C. If these microbes are indeed using MAOM C as an energy source, MAOM C gained by higher rates of POM decay and greater organic matter export to soil mineral surfaces may be offset by C losses from MAOM decomposition.

Across large spatial scales, the effects of climate on MAOM C may also be modified by concurrent changes in 1) soil weathering rate and, subsequently, the availability of poorly crystalline mineral phases (Slessarev et al., 2022), or 2) primary productivity, which controls the rate of organic matter inputs to soil. While we found that plot productivity, represented by tree basal area, was not related to the climate decomposition index of our study sites ($F_{1,46}$= 0.047; p =0.83), soil in warmer sites did have the largest concentrations of FeOx ($F_{1,46}$= 13.44; $p < 0.001$). However, the concentration of MAOM C was negatively associated with climate decomposition index, despite these warmer sites having higher concentrations of FeOx, indicating suitable mineralogy for MAOM formation (Slessarev et al., 2022). Therefore, we suggest that climate-driven variation in SOM C concentrations in our study is not likely due to covarying effects of climate on soil mineralogy or organic matter production.

Carbon isotopes and MAOM decomposition and persistence

We expected MAOM carbon in warmer sites to have more enriched $\delta^{13}C$ and $\Delta^{14}C$ signatures due to the generally faster rates of microbial decomposition and C cycling with increasing mean annual temperature (Shi et al., 2020; Yang et al., 2014). Instead, we found a minor decrease in $\delta^{13}C$ with increasing CDI, and no effect of CDI on $\Delta^{14}C$ (Table 4; Figure S1). Further, $\delta^{13}C$ increased with the percentage of FeOx in our samples, though this trend was most evident at LENO, where the largest variation in FeOx was observed (Figure S1). Given the positive association between concentrations of MAOM C and N and FeOx, this pattern in $\delta^{13}C$ may be due to overall faster rates of microbial activity and opportunity for organo-mineral interactions at this site, where both climate and mineralogy are well-suited for MAOM formation. As has been noted in other studies, soil radiocarbon content across our study sites were not necessarily correlated with the factors that controlled the concentrations of C and N in SOM fractions (K. A. Heckman, Nave, et al., 2021; McFarlane et al., 2013). These patterns suggest that local conditions, perhaps land use history, hydrology, or soil disturbance, may be more important than climate, microbial communities or the availability of potential binding sites for explaining variation in MAOM turnover times within biomes. For example, the lowest $\Delta^{14}C$ values, indicating older MAOM C, were measured at DELA, a seasonally flooded bottomland forest, where, despite a high mean annual temperature, soil inundation likely limits decomposition and supports the persistence of MAOM C, while inhibiting the formation of new MAOM. Conversely, the high $\Delta^{14}C$ values at SERC may be due to regular mixing of new litter material into the mineral soil by the invasive earthworm *Lumbricus rubellus* (Crow et al., 2009). The radiocarbon content of the MAOM at other sites in our study was relatively consistent, with

most C reflecting a near modern origin, despite variation in climate and soil type. Though others have identified broad-scale patterns in soil $\Delta^{14}C$ corresponding with climate and soil mineralogy (Mathieu et al., 2015; Shi et al., 2020), it is likely that the variation in these factors among the sites used in our study was insufficient to demonstrate these effects.

The site-specific conditions that may have influenced MAOM carbon age in our study may be difficult to identify in broad-scale analyses of soil carbon age. Therefore, to accurately predict fine-scale variation in MAOM persistence, we suggest that individually-derived models of MAOM turnover based on local conditions that influence SOM decomposition rates are needed. Additionally, it is generally accepted that MAOM pools are heterogeneous in nature, with fast-cycling and slow-cycling components that are governed by distinct environmental conditions and inputs and likely vary in their chemical compositions (Neurath et al., 2021; Sokol et al., 2022). Therefore, it is possible that drivers of MAOM C and N concentrations in our sites also exert important controls on MAOM persistence in either the slow-cycling or fast-cycling fraction, but that these patterns were not detectable in our analysis of MAOM radiocarbon content. Further, because radiocarbon-based estimates of MAOM age represent the average persistence of both fast and slow-cycling MAOM fractions, the patterns observed here do not necessarily reflect the stability of the total MAOM pool across our study sites, but rather offer a general comparison of the average MAOM C turnover time.

Conclusion

We show that soil reactive iron content and climate were the best predictors of MAOM C and N concentrations in the upper mineral soils in eastern U.S. forests, but that tree mycorrhizal type influences the relative proportion of C and N in MAOM vs. POM. Additionally, climate

534 influenced the effect of tree mycorrhizal type on the relative proportion of N in SOM density
535 fractions, where forests dominated by ECM-associated trees stored relatively more soil N as
536 MAOM in colder climates, but less soil N as MAOM in warmer climates, when compared with
537 stands dominated by AM-associated trees. Radiocarbon content of the mineral-associated soil
538 fraction did not help explain potential mechanisms for the patterns we found in MAOM C and N
539 concentrations: we found that the MAOM fraction radiocarbon age was unrelated to soil
540 mineralogy, tree mycorrhizal type, or climate, suggesting that other factors operating at local
541 scales may be more important for explaining variation in MAOM turnover within biomes. These
542 results support recent findings that mycorrhizal fungi influence the distribution of soil C and N
543 among different SOM fractions, which vary in their vulnerability to decay and are thus critical
544 for predicting soil C and N dynamics in a changing climate. Given the interactive effects of
545 climate and tree mycorrhizal type on the proportion of soil N in MAOM vs. POM, we encourage
546 models of the controls on SOM C and N pools across large spatial scales to more directly
547 account for how the primary drivers of MAOM and POM pools vary across climate gradients.
548

549 **Acknowledgements**

550 The National Ecological Observatory Network is a program sponsored by the National Science
551 Foundation and operated under cooperative agreement by Battelle. This material uses samples
552 collected as part of the NEON Program. The authors thank Kelsey Yule for assisting with the
553 selection and acquisition of soil samples needed to conduct this work. We further thank
554 Elizabeth Huenupi-Pena for assistance with laboratory analyses. Authors declare no conflicts of
555 interest.
556

Funding

A.K.L undertook this research while supported by the National Science Foundation Postdoctoral Research Fellowship in Biology (award number 2010724). Work at LLNL was supported by the U.S. Department of Energy (DOE), Office of Biological and Environmental Research (BER), Genomic Science Program Lawrence Livermore National Laboratory (LLNL) 'Microbes Persist' Soil Microbiome Scientific Focus Area SCW1632, under the auspices of the DOE, Contract DE-AC52-07NA27344.

Author contributions

A.K.L., R.P.P., and J.P.R. conceived of and designed the study, R.P.P. and J.P.R. provided institutional support for analyses, A.K.L. and K.J.M. conducted laboratory analyses, A.K.L. wrote the manuscript, and all authors contributed substantially to edits and improvements.

Data Availability Statement

Woody vegetation data (DP1.10098.001) and leaf litter production and chemistry data (DP1.10033.001) for the NEON sites used in this study are available on the NEON Data Portal (https://data.neonscience.org/). Other data and code for the analyses generated by this work are available at https://github.com/ashleylang/NEON_MAOM.

References

Adair, E. C., Parton, W. J., del Grosso, S. J., Silver, W. L., Harmon, M. E., Hall, S. A., Burke, I. C., & Hart, S. C. (2008). Simple three-pool model accurately describes patterns of long-term litter decomposition in diverse climates. *Global Change Biology*, *14*(11), 2636–2660.

580 Amelung, W., Bossio, D., de Vries, W., Kögel-Knabner, I., Lehmann, J., Amundson, R., Bol, R.,
581 Collins, C., Lal, R., Leifeld, J., Minasny, B., Pan, G., Paustian, K., Rumpel, C., Sanderman,
582 J., van Groenigen, J. W., Mooney, S., van Wesemael, B., Wander, M., & Chabbi, A. (2020).
583 Towards a global-scale soil climate mitigation strategy. *Nature Communications*, *11*(1), 1–
584 10.
585 Angst, G., Mueller, K. E., Nierop, K. G. J., & Simpson, M. J. (2021). Plant- or microbial-
586 derived? A review on the molecular composition of stabilized soil organic matter. *Soil*
587 *Biology & Biochemistry*, *156*, 108189.
588 Bates, D., Mächler, M., Bolker, B., & Walker, S. (2015). Fitting Linear Mixed-Effects Models
589 Using lme4. *Journal of Statistical Software, Articles*, *67*(1), 1–48.
590 Bossio, D. A., Cook-Patton, S. C., Ellis, P. W., Fargione, J., Sanderman, J., Smith, P., Wood, S.,
591 Zomer, R. J., von Unger, M., Emmer, I. M., & Griscom, B. W. (2020). The role of soil
592 carbon in natural climate solutions. *Nature Sustainability*, *3*(5), 391–398.
593 Broek, T. A. B., Ognibene, T. J., McFarlane, K. J., Moreland, K. C., Brown, T. A., & Bench, G.
594 (2021). Conversion of the LLNL/CAMS 1 MV biomedical AMS system to a semi-
595 automated natural abundance 14C spectrometer: system optimization and performance
596 evaluation. *Nuclear Instruments & Methods in Physics Research. Section B, Beam*
597 *Interactions with Materials and Atoms*, *499*, 124–132.
598 Carteron, A., Beigas, M., Joly, S., Turner, B. L., & Laliberté, E. (2020). Temperate Forests
599 Dominated by Arbuscular or Ectomycorrhizal Fungi Are Characterized by Strong Shifts
600 from Saprotrophic to Mycorrhizal Fungi with Increasing Soil Depth. *Microbial Ecology*.
601 https://doi.org/10.1007/s00248-020-01540-7
602 Catford, J. A., Wilson, J. R. U., Pyšek, P., Hulme, P. E., & Duncan, R. P. (2022). Addressing

603 context dependence in ecology. *Trends in Ecology & Evolution*, *37*(2), 158–170.
604 Cheeke, T. E., Phillips, R. P., Brzostek, E. R., Rosling, A., Bever, J. D., & Fransson, P. (2016).
605 Dominant mycorrhizal association of trees alters carbon and nutrient cycling by selecting
606 for microbial groups with distinct enzyme function. *The New Phytologist*, *214*(1), 432–442.
607 Cornelissen, J., Aerts, R., Cerabolini, B., Werger, M., & van der Heijden, M. (2001). Carbon
608 cycling traits of plant species are linked with mycorrhizal strategy. *Oecologia*, *129*(4), 611–
609 619.
610 Cotrufo, M. F., Ranalli, M. G., Haddix, M. L., Six, J., & Lugato, E. (2019). Soil carbon storage
611 informed by particulate and mineral-associated organic matter. *Nature Geoscience*, *12*(12),
612 989–994.
613 Cotrufo, M. F., Wallenstein, M. D., Boot, C. M., Denef, K., & Paul, E. (2013). The Microbial
614 Efficiency-Matrix Stabilization (MEMS) framework integrates plant litter decomposition
615 with soil organic matter stabilization: Do labile plant inputs form stable soil organic matter?
616 *Global Change Biology*, *19*(4), 988–995.
617 Craig, M. E., Geyer, K. M., Beidler, K. V., Brzostek, E. R., Frey, S. D., Stuart Grandy, A.,
618 Liang, C., & Phillips, R. P. (2022). Fast-decaying plant litter enhances soil carbon in
619 temperate forests but not through microbial physiological traits. *Nature Communications*,
620 *13*(1), 1229.
621 Craig, M. E., Turner, B. L., Liang, C., Clay, K., Johnson, D. J., & Phillips, R. P. (2018). Tree
622 mycorrhizal type predicts within-site variability in the storage and distribution of soil
623 organic matter. *Global Change Biology*, *24*(8), 3317–3330.
624 Crow, S. E., Lajtha, K., Filley, T. R., Swanston, C. W., Bowden, R. D., & Caldwell, B. A.
625 (2009). Sources of plant-derived carbon and stability of organic matter in soil: implications

626 for global change. *Global Change Biology*, *15*(8), 2003–2019.
627 Fernandez, C. W., Langley, J. A., Chapman, S., McCormack, M. L., & Koide, R. T. (2016). The
628 decomposition of ectomycorrhizal fungal necromass. *Soil Biology & Biochemistry*, *93*, 38–
629 49.
630 Fitch, A. A., Lang, A., Whalen, E., & Geyer, K. M. (2020). Fungal community, not substrate
631 quality, drives soil microbial function in Northeast temperate forests. *Frontiers in Forests*
632 *and*.
633 Fossum, C., Estera-Molina, K. Y., Yuan, M., Herman, D. J., Chu-Jacoby, I., Nico, P. S.,
634 Morrison, K. D., Pett-Ridge, J., & Firestone, M. K. (2022). Belowground allocation and
635 dynamics of recently fixed plant carbon in a California annual grassland. *Soil Biology &*
636 *Biochemistry*, *165*, 108519.
637 Frey, S. D. (2019). Mycorrhizal Fungi as Mediators of Soil Organic Matter Dynamics. *Annual*
638 *Review of Ecology, Evolution, and Systematics*, *50*(1), 237–259.
639 Haddix, M. L., Gregorich, E. G., Helgason, B. L., Janzen, H., Ellert, B. H., & Francesca Cotrufo,
640 M. (2020). Climate, carbon content, and soil texture control the independent formation and
641 persistence of particulate and mineral-associated organic matter in soil. *Geoderma*, *363*,
642 114160.
643 Hakkenberg, C. R., Goetz, S. J., & Gillespie, T. (2021). Climate mediates the relationship
644 between plant biodiversity and forest structure across the United States. *Global Ecology and*
645 *Biogeography: A Journal of Macroecology*, *30*(11), 2245–2258.
646 Heckman, K. A., Lawrence, C. R., Harden, J. W., Crate, J., & Swanston, C. (2015). *Ironing out*
647 *the details of soil organic matter cycling: The unique role of Fe-bearing minerals in*
648 *regulating organic matter transformation in soils*. *2015*, B32C – 01.

649 Heckman, K. A., Nave, L. E., Bowman, M., Gallo, A., Hatten, J. A., Matosziuk, L. M.,
650 Possinger, A. R., SanClements, M., Strahm, B. D., Weiglein, T. L., Rasmussen, C., &
651 Swanston, C. W. (2021). Divergent controls on carbon concentration and persistence
652 between forests and grasslands of the conterminous US. *Biogeochemistry*, *156*(1), 41–56.
653 Heckman, K. A., Swanston, C. W., Torn, M. S., Hanson, P. J., Nave, L. E., Porras, R. C., Mishra,
654 U., & Bill, M. (2021). Soil organic matter is principally root derived in an Ultisol under oak
655 forest. *Geoderma*, *403*, 115385.
656 Heckman, K., Hicks Pries, C. E., Lawrence, C. R., Rasmussen, C., Crow, S. E., Hoyt, A. M., von
657 Fromm, S. F., Shi, Z., Stoner, S., McGrath, C., Beem-Miller, J., Berhe, A. A., Blankinship,
658 J. C., Keiluweit, M., Marín-Spiotta, E., Monroe, J. G., Plante, A. F., Schimel, J., Sierra, C.
659 A., … Wagai, R. (2022). Beyond bulk: Density fractions explain heterogeneity in global
660 soil carbon abundance and persistence. *Global Change Biology*, *28*(3), 1178–1196.
661 Heckman, K., Lawrence, C. R., & Harden, J. W. (2018). A sequential selective dissolution
662 method to quantify storage and stability of organic carbon associated with Al and Fe
663 hydroxide phases. *Geoderma*, *312*, 24–35.
664 Hinckley, E.-L. S., Bonan, G. B., Bowen, G. J., Colman, B. P., Duffy, P. A., Goodale, C. L.,
665 Houlton, B. Z., Marín-Spiotta, E., Ogle, K., Ollinger, S. V., Paul, E. A., Vitousek, P. M.,
666 Weathers, K. C., & Williams, D. G. (2016). The soil and plant biogeochemistry sampling
667 design for The National Ecological Observatory Network. *Ecosphere* , *7*(3), e01234.
668 Hoffland, E., Kuyper, T. W., Comans, R. N. J., & Creamer, R. E. (2020). Eco-functionality of
669 organic matter in soils. *Plant and Soil*, *455*(1), 1–22.
670 Huang, W., van Bodegom, P. M., Declerck, S., Heinonsalo, J., Cosme, M., Viskari, T., Liski, J.,
671 & Soudzilovskaia, N. A. (2022). Mycelium chemistry differs markedly between

ectomycorrhizal and arbuscular mycorrhizal fungi. *Communications Biology*, *5*(1), 398.

Jevon, F. V., & Lang, A. K. (2022). Tree biomass allocation differs by mycorrhizal association. *Ecology*, *103*(6), e3688.

Jilling, A., Keiluweit, M., Contosta, A. R., Frey, S., Schimel, J., Schnecker, J., Smith, R. G., Tiemann, L., & Grandy, A. S. (2018). Minerals in the rhizosphere: overlooked mediators of soil nitrogen availability to plants and microbes. *Biogeochemistry*, *139*(2), 103–122.

Jilling, A., Keiluweit, M., Gutknecht, J. L. M., & Grandy, A. S. (2021). Priming mechanisms providing plants and microbes access to mineral-associated organic matter. *Soil Biology & Biochemistry*, *158*(108265), 108265.

Jones, A. R., Sanderman, J., Allen, D., Dalal, R., & Schmidt, S. (2015). Subtropical giant podzol chronosequence reveals that soil carbon stabilisation is not governed by litter quality. *Biogeochemistry*, *124*(1), 205–217.

Keiluweit, M., Bougoure, J. J., Nico, P. S., Pett-Ridge, J., Weber, P. K., & Kleber, M. (2015). Mineral protection of soil carbon counteracted by root exudates. *Nature Climate Change*, *5*(6), 588–595.

Keiluweit, M., Bougoure, J. J., Zeglin, L. H., Myrold, D. D., Weber, P. K., Pett-Ridge, J., Kleber, M., & Nico, P. S. (2012). Nano-scale investigation of the association of microbial nitrogen residues with iron (hydr)oxides in a forest soil O-horizon. *Geochimica et Cosmochimica Acta*, *95*, 213–226.

Keller, A. B., Brzostek, E. R., Craig, M. E., Fisher, J. B., & Phillips, R. P. (2021). Root-derived inputs are major contributors to soil carbon in temperate forests, but vary by mycorrhizal type. *Ecology Letters*, *24*(4), 626–635.

Keller, A. B., & Phillips, R. P. (2019). Leaf litter decay rates differ between mycorrhizal groups

695 in temperate, but not tropical, forests. *The New Phytologist*, *222*(1), 556–564.
696 Kleber, M., Mikutta, R., Torn, M. S., & Jahn, R. (2005). Poorly crystalline mineral phases
697 protect organic matter in acid subsoil horizons. *European Journal of Soil Science*, *0*(0),
698 050912034650054.
699 Kögel-Knabner, I., Guggenberger, G., Kleber, M., Kandeler, E., Kalbitz, K., Scheu, S.,
700 Eusterhues, K., & Leinweber, P. (2008). Organo-mineral associations in temperate soils:
701 Integrating biology, mineralogy, and organic matter chemistry. *Journal of Plant Nutrition*
702 *and Soil Science*, *171*(1), 61–82.
703 Kramer, M. G., & Chadwick, O. A. (2018). Climate-driven thresholds in reactive mineral
704 retention of soil carbon at the global scale. *Nature Climate Change*.
705 https://www.nature.com/articles/s41558-018-0341-4
706 Lal, R. (2004). Soil carbon sequestration impacts on global climate change and food security.
707 *Science* , *304*(5677), 1623–1627.
708 Lambers, H., Raven, J. A., Shaver, G. R., & Smith, S. E. (2008). Plant nutrient-acquisition
709 strategies change with soil age. *Trends in Ecology & Evolution*, *23*(2), 95–103.
710 Lehmann, J., & Kleber, M. (2015). The contentious nature of soil organic matter. *Nature*, 0–9.
711 Liang, C., Amelung, W., Lehmann, J., & Kästner, M. (2019). Quantitative assessment of
712 microbial necromass contribution to soil organic matter. *Global Change Biology*, *25*(11),
713 3578–3590.
714 Lloyd, J., & Taylor, J. A. (1994). On the Temperature Dependence of Soil Respiration.
715 *Functional Ecology*, *8*(3), 315–323.
716 Lovett, G. M., Goodale, C. L., & Ollinger, S. V. (2018). Nutrient retention during ecosystem
717 succession: a revised conceptual model. *Frontiers in Ecology and the Environment*, *16*(9),

532–538.

Lugato, E., Lavallee, J. M., Haddix, M. L., Panagos, P., & Francesca Cotrufo, M. (2021). Different climate sensitivity of particulate and mineral-associated soil organic matter. *Nature Geoscience*, *14*(5), 295–300.

Lunch, C., Laney, C., Mietkiewicz, N., Sokol, E., Cawley, K., & NEON (National Ecological Observatory Network). (2021). *neonUtilities: Utilities for Working with NEON Data*. https://CRAN.R-project.org/package=neonUtilities

Mathieu, J. A., Hatté, C., Balesdent, J., & Parent, É. (2015). Deep soil carbon dynamics are driven more by soil type than by climate: a worldwide meta-analysis of radiocarbon profiles. *Global Change Biology*, *21*(11), 4278–4292.

McFarlane, K. J., Torn, M. S., Hanson, P. J., Porras, R. C., Swanston, C. W., Callaham, M. A., Jr, & Guilderson, T. P. (2013). Comparison of soil organic matter dynamics at five temperate deciduous forests with physical fractionation and radiocarbon measurements. *Biogeochemistry*, *112*(1-3), 457–476.

Mikutta, R., Kleber, M., Torn, M. S., & Jahn, R. (2006). Stabilization of soil organic matter: Association with minerals or chemical recalcitrance? *Biogeochemistry*, *77*(1), 25–56.

Mikutta, R., Turner, S., Schippers, A., Gentsch, N., Meyer-Stüve, S., Condron, L. M., Peltzer, D. A., Richardson, S. J., Eger, A., Hempel, G., Kaiser, K., Klotzbücher, T., & Guggenberger, G. (2019). Microbial and abiotic controls on mineral-associated organic matter in soil profiles along an ecosystem gradient. *Scientific Reports*, *9*(1), 10294.

Moore, J. A. M., Jiang, J., Patterson, C. M., Mayes, M. A., Wang, G., & Classen, A. T. (2015). Interactions among roots, mycorrhizas and free-living microbial communities differentially impact soil carbon processes. *The Journal of Ecology*, *103*(6), 1442–1453.

741 Nave, L. E., Bowman, M., Gallo, A., Hatten, J. A., Heckman, K. A., Matosziuk, L., Possinger,
742 A. R., SanClements, M., Sanderman, J., Strahm, B. D., Weiglein, T. L., & Swanston, C. W.
743 (2021). Patterns and predictors of soil organic carbon storage across a continental-scale
744 network. *Biogeochemistry*, *156*(1), 75–96.
745 NEON. (2022a). *Litterfall and fine woody debris production and chemistry. (DP1.10033.001). National Ecological Observatory Network* [Data set]. https://doi.org/10.48443/b2qt-7z79
747 NEON. (2022b). *Vegetation structure (DP1.10098.001). National Ecological Observatory*
748 *Network* [Data set]. National Ecological Observatory Network (NEON).
749 https://doi.org/10.48443/RE8N-TN87
750 Neurath, R. A., Pett-Ridge, J., Chu-Jacoby, I., Herman, D., Whitman, T., Nico, P. S., Lipton, A.
751 S., Kyle, J., Tfaily, M. M., Thompson, A., & Firestone, M. K. (2021). Root Carbon
752 Interaction with Soil Minerals Is Dynamic, Leaving a Legacy of Microbially Derived
753 Residues. *Environmental Science & Technology*, *55*(19), 13345–13355.
754 Paustian, K., Larson, E., Kent, J., Marx, E., & Swan, A. (2019). Soil C Sequestration as a
755 Biological Negative Emission Strategy. *Frontiers in Climate*, *1*.
756 https://doi.org/10.3389/fclim.2019.00008
757 Pellitier, P. T., & Zak, D. R. (2018). Ectomycorrhizal fungi and the enzymatic liberation of
758 nitrogen from soil organic matter: why evolutionary history matters. *The New Phytologist*,
759 *217*(1), 68–73.
760 PRISM Climate Group, Oregon State University. (n.d.). *Parameter-elevation Regressions on*
761 *Independent Slopes Model (PRISM) dataset* [Data set]. Retrieved November 8, 2021, from
762 www.prism.oregonstate.edu
763 Rasmussen, C., Heckman, K., Wieder, W. R., Keiluweit, M., Lawrence, C. R., Berhe, A. A.,

764 Blankinship, J. C., Crow, S. E., Druhan, J. L., Hicks Pries, C. E., Marin-Spiotta, E., Plante,
765 A. F., Schädel, C., Schimel, J. P., Sierra, C. A., Thompson, A., & Wagai, R. (2018). Beyond
766 clay: towards an improved set of variables for predicting soil organic matter content.
767 *Biogeochemistry*, *137*(3), 297–306.
768 Scharlemann, J. P. W., Tanner, E. V. J., Hiederer, R., & Kapos, V. (2014). Global soil carbon:
769 understanding and managing the largest terrestrial carbon pool. *Carbon Management*, *5*(1),
770 81–91.
771 Schöning, I., Knicker, H., & Kögel-Knabner, I. (2005). Intimate association between O/N-alkyl
772 carbon and iron oxides in clay fractions of forest soils. *Organic Geochemistry*, *36*(10),
773 1378–1390.
774 Shi, Z., Allison, S. D., He, Y., Levine, P. A., Hoyt, A. M., Beem-Miller, J., Zhu, Q., Wieder, W.
775 R., Trumbore, S., & Randerson, J. T. (2020). The age distribution of global soil carbon
776 inferred from radiocarbon measurements. *Nature Geoscience*, *13*(8), 555–559.
777 Singavarapu, B., Beugnon, R., Bruelheide, H., Cesarz, S., Du, J., Eisenhauer, N., Guo, L.-D.,
778 Nawaz, A., Wang, Y., Xue, K., & Wubet, T. (2022). Tree mycorrhizal type and tree
779 diversity shape the forest soil microbiota. *Environmental Microbiology*, *24*(9), 4236–4255.
780 Slessarev, E. W., Chadwick, O. A., Sokol, N. W., Nuccio, E. E., & Pett-Ridge, J. (2022). Rock
781 weathering controls the potential for soil carbon storage at a continental scale.
782 *Biogeochemistry*, *157*(1), 1–13.
783 Sokol, N. W., Sanderman, J., & Bradford, M. A. (2018). Pathways of mineral-associated soil
784 organic matter formation: Integrating the role of plant carbon source, chemistry, and point
785 of entry. *Global Change Biology*, *25*(1), 12–24.
786 Sokol, N. W., Whalen, E. D., Jilling, A., Kallenbach, C., Pett-Ridge, J., & Georgiou, K. (2022).

Global distribution, formation and fate of mineral-associated soil organic matter under a changing climate: A trait-based perspective. *Functional Ecology*. https://doi.org/10.1111/1365-2435.14040

Sollins, P., Kramer, M. G., Swanston, C., Lajtha, K., Filley, T., Aufdenkampe, A. K., Wagai, R., & Bowden, R. D. (2009). Sequential density fractionation across soils of contrasting mineralogy: evidence for both microbial- and mineral-controlled soil organic matter stabilization. *Biogeochemistry*, *96*(1), 209–231.

Soranno, P. A., Cheruvelil, K. S., Bissell, E. G., Bremigan, M. T., Downing, J. A., Fergus, C. E., Filstrup, C. T., Henry, E. N., Lottig, N. R., Stanley, E. H., Stow, C. A., Tan, P.-N., Wagner, T., & Webster, K. E. (2014). Cross-scale interactions: quantifying multi-scaled cause–effect relationships in macrosystems. *Frontiers in Ecology and the Environment*, *12*(1), 65–73.

Stuiver, M., & Polach, H. A. (1977). Discussion Reporting of 14C Data. *Radiocarbon*, *19*(3), 355–363.

Swanston, C. W., Torn, M. S., Hanson, P. J., Southon, J. R., Garten, C. T., Hanlon, E. M., & Ganio, L. (2005). Initial characterization of processes of soil carbon stabilization using forest stand-level radiocarbon enrichment. *Geoderma*, *128*(1), 52–62.

Swenson, T. L., Bowen, B. P., Nico, P. S., & Northen, T. R. (2015). Competitive sorption of microbial metabolites on an iron oxide mineral. *Soil Biology & Biochemistry*, *90*, 34–41.

Tedersoo, L., & Bahram, M. (2019). Mycorrhizal types differ in ecophysiology and alter plant nutrition and soil processes. *Biological Reviews of the Cambridge Philosophical Society*, *94*(5), 1857–1880.

Tedersoo, L., Bahram, M., Cajthaml, T., Põlme, S., Hiiesalu, I., Anslan, S., Harend, H., Buegger, F., Pritsch, K., Koricheva, J., & Abarenkov, K. (2016). Tree diversity and species identity

effects on soil fungi, protists and animals are context dependent. *The ISME Journal*, *10*(2), 346–362.

Torn, M. S., Trumbore, S. E., Chadwick, O. A., Vitousek, P. M., & Hendricks, D. M. (1997). Mineral control of soil organic carbon storage and turnover. *Nature*, *389*(6647), 170–173.

Trumbore, S., Gaudinski, J. B., Hanson, P. J., & Southon, J. R. (2002). Quantifying ecosystem-atmosphere carbon exchange with a 14C label. *Eos*, *83*(24), 265.

USDA, NRCS. National Plant Data Team. (2021). *The PLANTS Database* [Data set]. http://plants.usda.gov

Waring, B. G., Sulman, B. N., Reed, S., Smith, A. P., Averill, C., Creamer, C. A., Cusack, D. F., Hall, S. J., Jastrow, J. D., Jilling, A., Kemner, K. M., Kleber, M., Liu, X.-J. A., Pett-Ridge, J., & Schulz, M. (2020). From pools to flow: The PROMISE framework for new insights on soil carbon cycling in a changing world. *Global Change Biology*, *26*(12), 6631–6643.

Weng, Y.-T., Wang, C.-C., Chiang, C.-C., Tsai, H., Song, Y.-F., Huang, S.-T., & Liang, B. (2018). In situ evidence of mineral physical protection and carbon stabilization revealed by nanoscale 3-D tomography. *Biogeosciences* , *15*(10), 3133–3142.

Yang, W., Magid, J., Christensen, S., Rønn, R., Ambus, P., & Ekelund, F. (2014). Biological 12C–13C fractionation increases with increasing community-complexity in soil microcosms. *Soil Biology & Biochemistry*, *69*, 197–201.

Yu, W., Huang, W., Weintraub-Leff, S. R., & Hall, S. J. (2022). Where and why do particulate organic matter (POM) and mineral-associated organic matter (MAOM) differ among diverse soils? *Soil Biology & Biochemistry*, *172*, 108756.

Table 1. Location of study sites with mean climate conditions, soil order, and dominant AM and ECM tree species in the selected study plots by basal area

Site	Location	MAT (°C)	MAP (mm)	Dominant Soil Order	Dominant AM Tree Species	Dominant ECM Tree Species
Treehaven (TREE)	Lincoln County, WI 45.49369 °N -89.58571 °W	4.8	797	Spodosol	*Acer rubrum* *Acer saccharum*	*Pinus strobus* *Picea mariana*
Bartlett Experimental Forest (BART)	Carroll County, NH 44.063889 °N -71.287375 °W	6.2	1325	Spodosol	*Acer rubrum* *Fraxinus americana*	*Fagus grandifolia* *Tsuga canadensis*
Harvard Forest (HARV)	Worcester County, MA 42.53691 °N -72.17265 °W	7.4	1199	Inceptisol	*Acer rubrum* *Fraxinus americana*	*Tsuga canadensis* *Quercus rubra*
Smithsonian Environmental Research Center (SERC)	Anne Arundel County, MD 38.890131 °N -76.560014 °W	13.6	1075	Ultisol	*Liriodendron tulipifera* *Liquidambar styraciflua*	*Quercus alba* *Fagus grandifolia*
Oak Ridge National Lab (ORNL)	Anderson County, TN 35.964128 °N -84.282588 °W	14.4	1340	Ultisol	*Liriodendron tulipifera* *Acer rubrum*	*Quercus alba* *Quercus montana*
Dead Lake (DELA)	Greene County, AL 32.541727 °N	17.6	1372	Ultisol	*Acer rubrum* *Celtis laevigata*	*Pinus taeda* *Quercus michauxii*

	-87.803877 °W					
Lenoir Landing (LENO)	Choctaw County, AL 31.853861 °N -88.161181 °W	18.1	1386	Inceptisol	*Liquidambar styraciflua* *Platanus occidentalis*	*Quercus pagoda* *Quercus laurifolia*

Table 2: Effects of mycorrhizal dominance (% ECM basal area), climate decomposition index (CDI), soil oxalate-extractable iron content (FeOx) and the interaction between mycorrhizal dominance and CDI on the proportions of total soil C and N in each SOM fraction, and the concentrations of fPOM, oPOM, and MAOM C and N in mineral soil (mg C within each fraction per gram of bulk soil) from plots located within seven forests in the National Ecological Observatory Network (NEON). Interactions terms were only included in final models when they were found to significantly influence SOM fractions. Standardized estimates are presented to allow comparison of the strengths of different drivers within models. Standardized standard errors follow in parentheses. Statistical significance indicates with asterisks: *: $p< 0.05$ **:$p<0.001$. For mycorrhizal dominance, a negative estimate reflects lower values of the response variable with increasing ECM tree dominance. Site included as a random intercept; for random effect variance see Table S2.

SOM fraction	***Predictor***	**Proportion of C** Std β (Std SE)	**Concentration of C** Std β (Std SE)	**Proportion of N** Std β (Std SE)	**Concentration of N** Std β (Std SE)
fPOM	(Intercept)	-0.00 (0.13)**	-0.01 (0.22)*	0.00 (0.12)**	-0.01 (0.21)**
	% ECM	0.28 (0.13)*	0.16 (0.12)	0.20 (0.13)	0.09 (0.12)
	CDI	-0.14 (0.15)	-0.48 (0.23)*	-0.40 (0.14)*	-0.49 (0.23)*
	FeOx	-0.50 (0.15)*	0.08 (0.16)	-0.24 (0.15)	0.01 (0.17)
	% ECM x CDI	*na*	*na*	*na*	*na*
oPOM	(Intercept)	0.00 (0.18)*	0.00 (0.19)*	-0.03 (0.13)	0.00 (0.20)*
	% ECM	0.33 (0.15)*	0.20 (0.13)	0.18 (0.14)	0.09 (0.13)
	CDI	0.12 (0.20)	-0.44 (0.21)*	-0.40 (0.16)*	-0.48 (0.22)*
	FeOx	-0.17 (0.18)	0.25 (0.17)	0.09 (0.16)	0.30 (0.18)
	% ECM x CDI	*na*	*na*	-0.28 (0.13)*	*na*
MAOM	(Intercept)	0.02 (0.14)**	0.00 (0.24)**	0.02 (0.11)	0.00 (0.18)*
	% ECM	-0.42 (0.13)*	-0.07 (0.10)	-0.23 (0.12)	-0.08 (0.11)
	CDI	0.02 (0.18)	-0.69 (0.25)*	0.50 (0.13)**	-0.32 (0.20)
	FeOx	0.50 (0.16)*	0.62 (0.15)**	0.09 (0.14)	0.88 (0.15)**
	% ECM x CDI	*na*	*na*	0.24 (0.11)*	*na*

Table 3. Effects of mycorrhizal dominance (% ECM basal area), climate decomposition index (CDI), and soil oxalate-extractable iron content (FeOx) on the ratio of carbon to nitrogen in each SOM density fraction from plots located within seven forests in the National Ecological Observatory Network (NEON). Standardized estimates are presented to allow comparison of the strengths of different drivers within models. Standardized standard errors follow in parentheses. Statistical significance indicates with asterisks: *: p< 0.05; **:p<0.001. For mycorrhizal dominance, a positive estimate reflects higher C:N with increasing ECM tree dominance. Site included as a random intercept; for random effect variance see Table S3.

		C:N
SOM fraction	***Predictor***	Std β (Std SE)
fPOM	(Intercept)	0.00 (0.17)**
	% ECM	0.41 (0.13)*
	CDI	0.12 (0.20)
	FeOx	-0.44 (0.17)*
oPOM	(Intercept)	0.00 (0.20)**
	% ECM	0.49 (0.13)**
	CDI	0.20 (0.22)
	FeOx	-0.23 (0.17)
MAOM	(Intercept)	0.00 (0.16)**
	% ECM	-0.17 (0.08)*
	CDI	-0.76 (0.17)**
	FeOx	-0.01 (0.11)

Table 4. Effects of mycorrhizal dominance (% ECM basal area), climate decomposition index (CDI), and soil oxalate-extractable iron content (FeOx) on MAOM $\delta^{13}C$ and $\Delta^{14}C$ from plots located within seven forests in the National Ecological Observatory Network (NEON). Standardized estimates are presented to allow comparison of the strengths of different drivers within models. Standardized standard errors follow in parentheses. Statistical significance indicated with asterisks: *: p< 0.05, **:p<0.001. For mycorrhizal dominance, a positive estimate reflects higher C:N with increasing ECM tree dominance. Site included as a random intercept; for random effect variance see Table S4.

	$\delta^{13}C$	**$\Delta^{14}C$**
Predictor	Std β (Std SE)	Std β (Std SE)
(Intercept)	0.00 (0.15)**	0.00 (0.16)
% ECM	-0.02 (0.15)	-0.09 (0.10)
CDI	-0.44 (0.20)*	-0.46 (0.41)
FeOx	0.64 (0.19)*	0.20 (0.14)

Supporting Information

Table S1. Proportions of tree basal area in each study plot from species associated with AM fungi, ECM fungi, and ericoid mycorrhizal (ERM) fungi.

Site	Plot Number	Proportion AM basal area	Proportion ECM basal area	Proportion ERM basal area
BART	32	0.46550818	0.53449182	0
BART	33	0.54740373	0.45259627	0
BART	34	0.32112415	0.67887585	0
BART	36	0.26891211	0.73108789	0
BART	40	0.82277588	0.17722412	0
BART	42	0.48449001	0.51550999	0
BART	71	0.40867927	0.59132073	0
DELA	1	0.93239645	0.06713732	0
DELA	2	0.54484444	0.45515556	0
DELA	4	0.66027181	0.33972819	0
DELA	14	0.15904082	0.84095918	0
DELA	37	0.34375437	0.65624563	0
DELA	38	0.72826961	0.27173039	0
DELA	41	1	0	0
HARV	1	0.07042541	0.92957459	0
HARV	4	0.66070745	0.3388294	0.00046315
HARV	10	0.06708706	0.93291294	0
HARV	16	0.50744061	0.48710657	0.00545281
HARV	21	0.359281	0.64016435	0.00055465
HARV	33	0.24117398	0.75882602	0
HARV	37	0.14561608	0.85438392	0

LENO	2	0.19986999	0.80013001	0
LENO	3	0.03369556	0.96630444	0
LENO	5	0.98372682	0.01627318	0
LENO	6	0.03273843	0.96726157	0
LENO	62	0.38208535	0.61791465	0
LENO	63	0.91260772	0.08739228	0
LENO	64	0.59565253	0.40434747	0
ORNL	3	0.36012176	0.63987824	0
ORNL	21	1	0	0
ORNL	29	0.45991508	0.53947474	0.00061018
ORNL	37	0.1857673	0.8142327	0
ORNL	43	0.28020524	0.71962444	0.00017032
ORNL	46	0.65660068	0.34326773	0.00013159
ORNL	49	0.87531323	0.12468677	0
SERC	1	1	0	0
SERC	2	0.50699133	0.49300867	0
SERC	3	0.91163537	0.08836463	0
SERC	5	0.77561132	0.22438868	0
SERC	45	0.3535429	0.64237524	0.00408186
SERC	47	0.41573443	0.58421976	4.58E-05
SERC	49	0.24009567	0.75990433	0
TREE	1	0.00127899	0.99872101	0
TREE	2	0.00101021	0.99898979	0
TREE	3	0.99899725	0.00100275	0
TREE	6	0.31994426	0.68005574	0
TREE	14	0.90922087	0.09077913	0
TREE	41	0.96148262	0.03851738	0

Table S2. Random effects of Site from models presented in Table 2: the concentrations and proportions of C and N in fPOM, oPOM, and MAOM from plots located within seven forests in the National Ecological Observatory Network (NEON)

	Proportion of C	**Concentration of C**	**Proportion of N**	**Concentration of N**
σ^2	0.00	36.91	0.00	0.13
ICC	0.05	0.43	0.00	0.26
Marginal R^2/Conditional R^2	0.357/ 0.392	0.359/0.635	0.429/0.429	0.484/0.618

Table S3. Random effects of Site from models presented in Table 3: C:N in fPOM, oPOM, and MAOM from plots located within seven forests in the National Ecological Observatory Network (NEON)

	fPOM C:N	**oPOM C:N**	**MAOM C:N**
σ^2	25.801	39.696	4.909
ICC	0.133	0.215	0.347
Marginal R^2/Conditional R^2	0.241/ 0.341	0.220/0.388	0.611/0.746

Table S4. Random effects of Site from models presented in Table 4: MAOM $\delta^{13}C$ and $\Delta^{14}C$ from plots located within seven forests in the National Ecological Observatory Network (NEON)

	MAOM $\delta^{13}C$	**MAOM $\Delta^{14}C$**
σ^2	0.16	584.64
ICC	0.02	0.73
Marginal R^2/Conditional R^2	0.227/0.239	0.094/0.754

Figure S1. Trends in MAOM carbon isotope ratios with climate decomposition index (CDI), % ECM tree basal area, and oxalate-extractable iron content from soil samples collected within six forests in the National Ecological Observatory Network (NEON). Solid lines indicate significant relationships at α=0.05. See Tables 4 and S4 for results of statistical models.